Electronic Supplementary Material (ESI) for CrystEngComm.

Supporting Information

Electro-deposition of Nickel-iron Nanoparticles on Flower-like $MnCo_2O_4$ Nanowires as an Efficient Bifunctional Electrocatalyst for Overall Water Splitting

Yu Lin[a] , Zhi Yang[a], Duanlin Cao[a], Yaqiong Gong[ab*]

a. School of Chemical Engineering and Technology, North University of China, Taiyuan 030051,

b. State Key Laboratory of Coordination Chemistry, Nanjing, Jiangsu 210046

E-mail: gyq@nuc.edu.cn

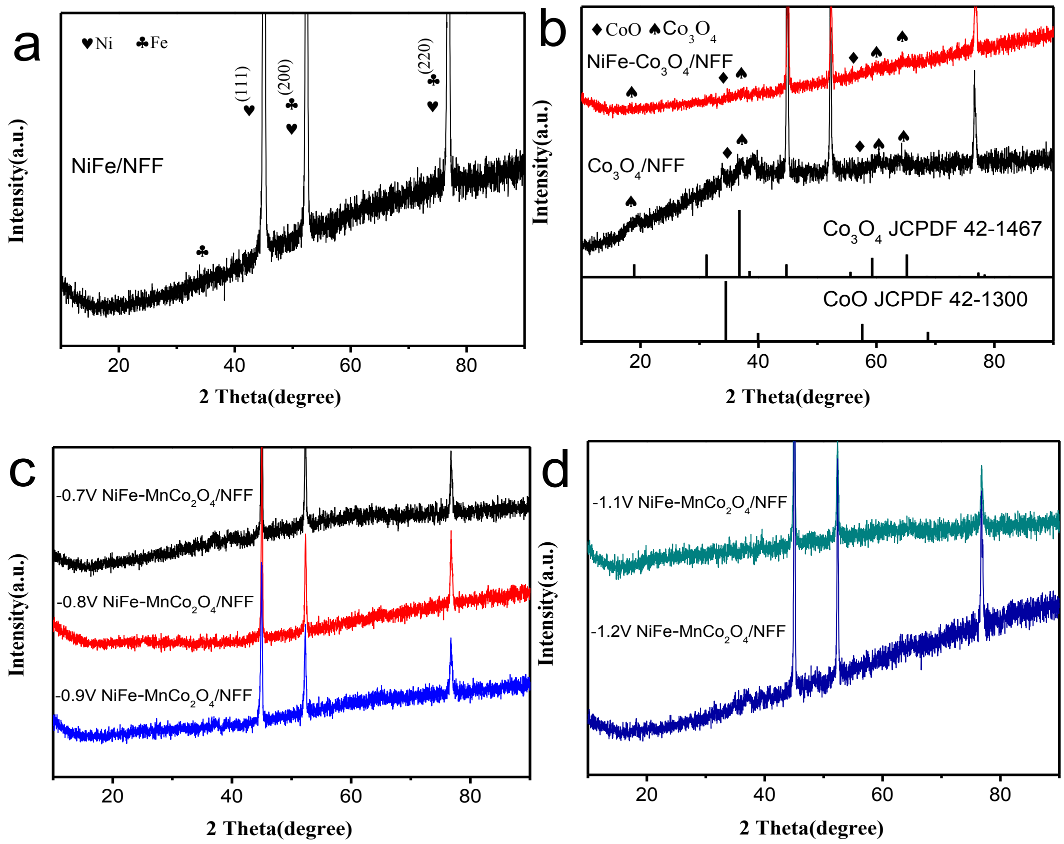

Fig. S1. XRD patterns of (a) NiFe/NFF (b) Co_3O_4/NFF and NiFe-Co_3O_4/NFF (c) -0.7V NiFe-$MnCo_2O_4$/NFF, -0.8V NiFe-$MnCo_2O_4$/NFF, and -0.9V NiFe-$MnCo_2O_4$/NFF (d) -1.1V NiFe-$MnCo_2O_4$/NFF and -1.2V NiFe-$MnCo_2O_4$/NFF.

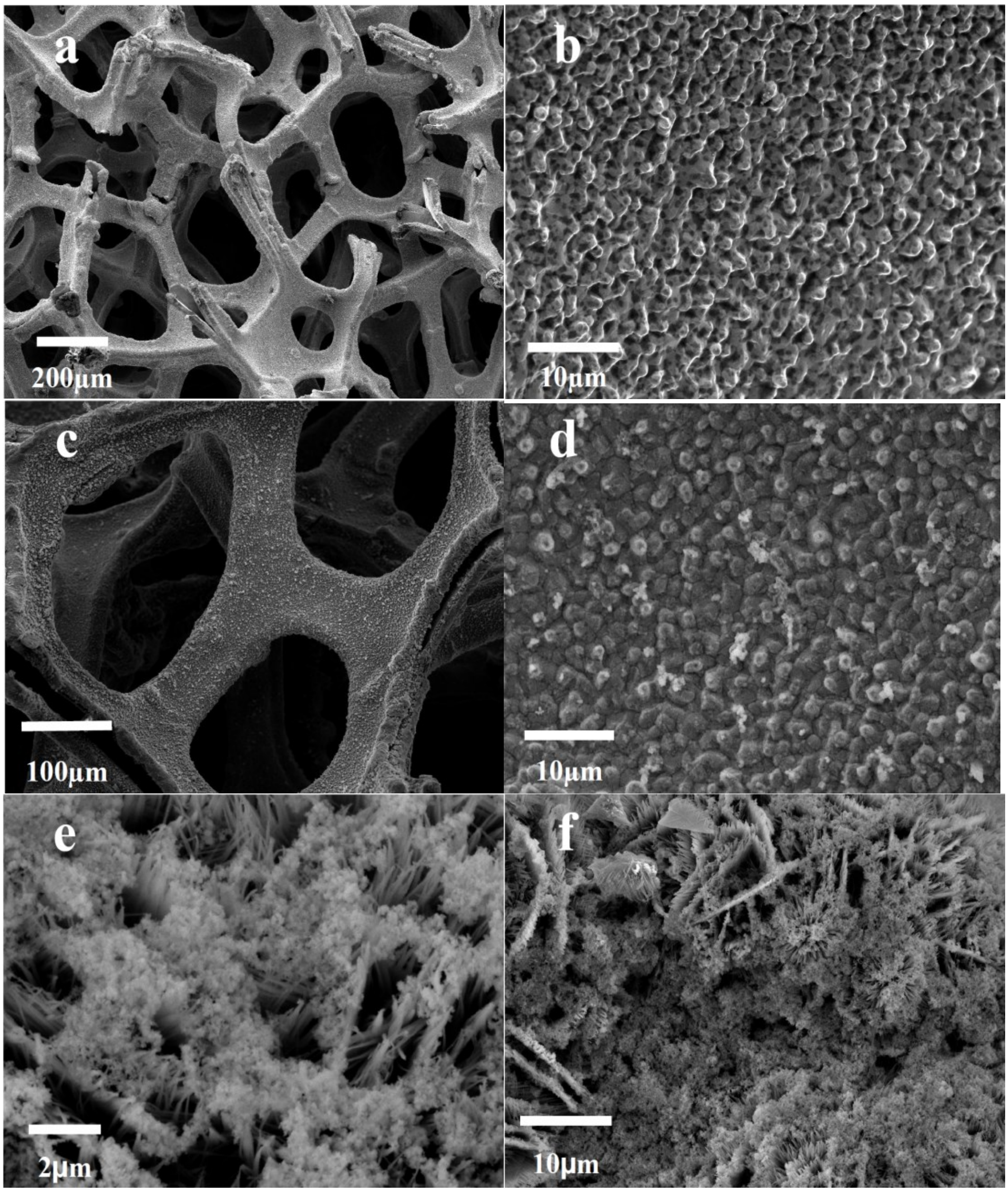

Fig. S2. SEM images of (a,b) NFF (c,d) NiFe/NFF (e,f) NiFe-Co_3O_4/NFF at different magnifications.

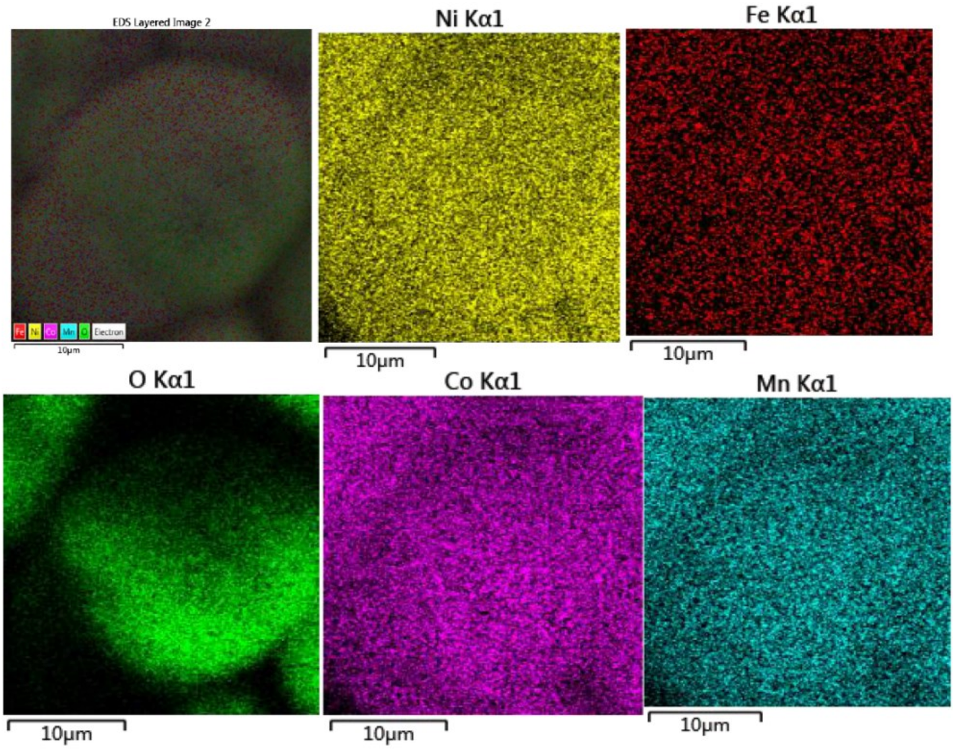

Fig. S3. Elemental mapping images of $MnCo_2O_4$/NFF nanoflower.

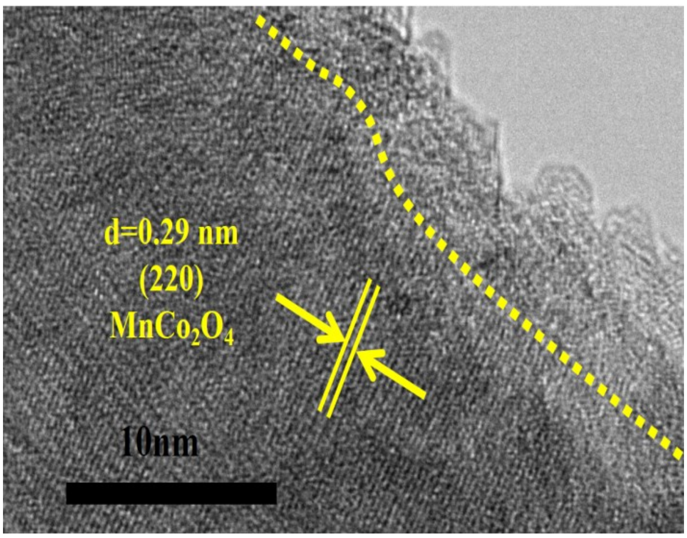

Fig. S4. HR-TEM images of NiFe-$MnCo_2O_4$/NFF.

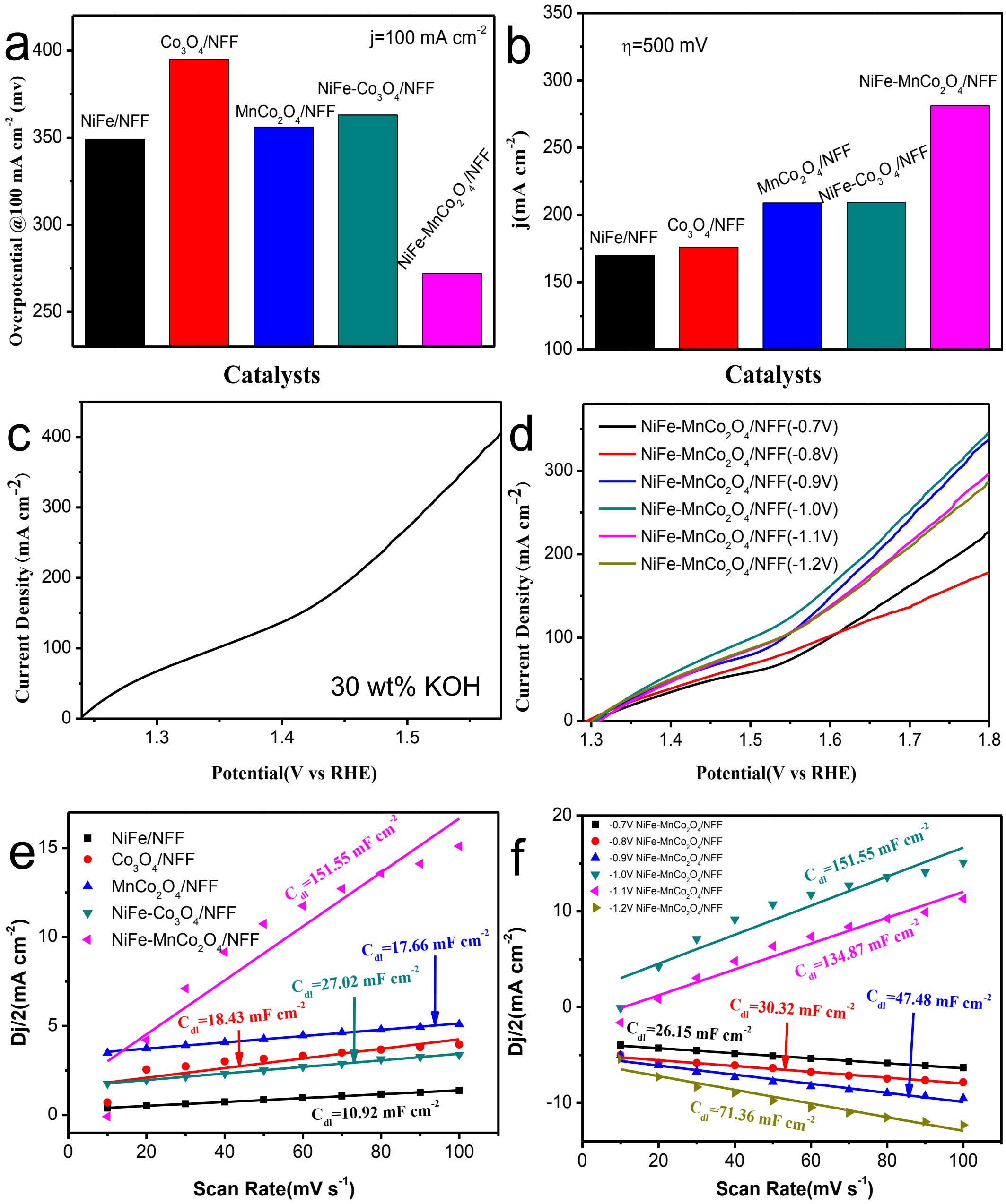

Fig. S5. OER (a) Overpotentials required for 100 mA cm^{-2}. (b) Current density at η = 500 mV for the different catalysts. (c) LSV curve for NiFe-$MnCo_2O_4$/NFF in 30 wt% KOH. (d) LSV curves for -0.7V NiFe-$MnCo_2O_4$/NFF, -0.8V NiFe-$MnCo_2O_4$/NFF, -0.9V NiFe-$MnCo_2O_4$/NFF, -1.0V NiFe-$MnCo_2O_4$/NFF, -1.1V NiFe-$MnCo_2O_4$/NFF, and -1.2V NiFe-$MnCo_2O_4$/NFF. (e) Capacitive currents of the catalysts with a scan rate of 10, 20, 30, 40, 50, 60, 70, 80, 90, and 100 mV s^{-1}. (f) Current density differences plotted against scan rates under a non-Faradaic range.

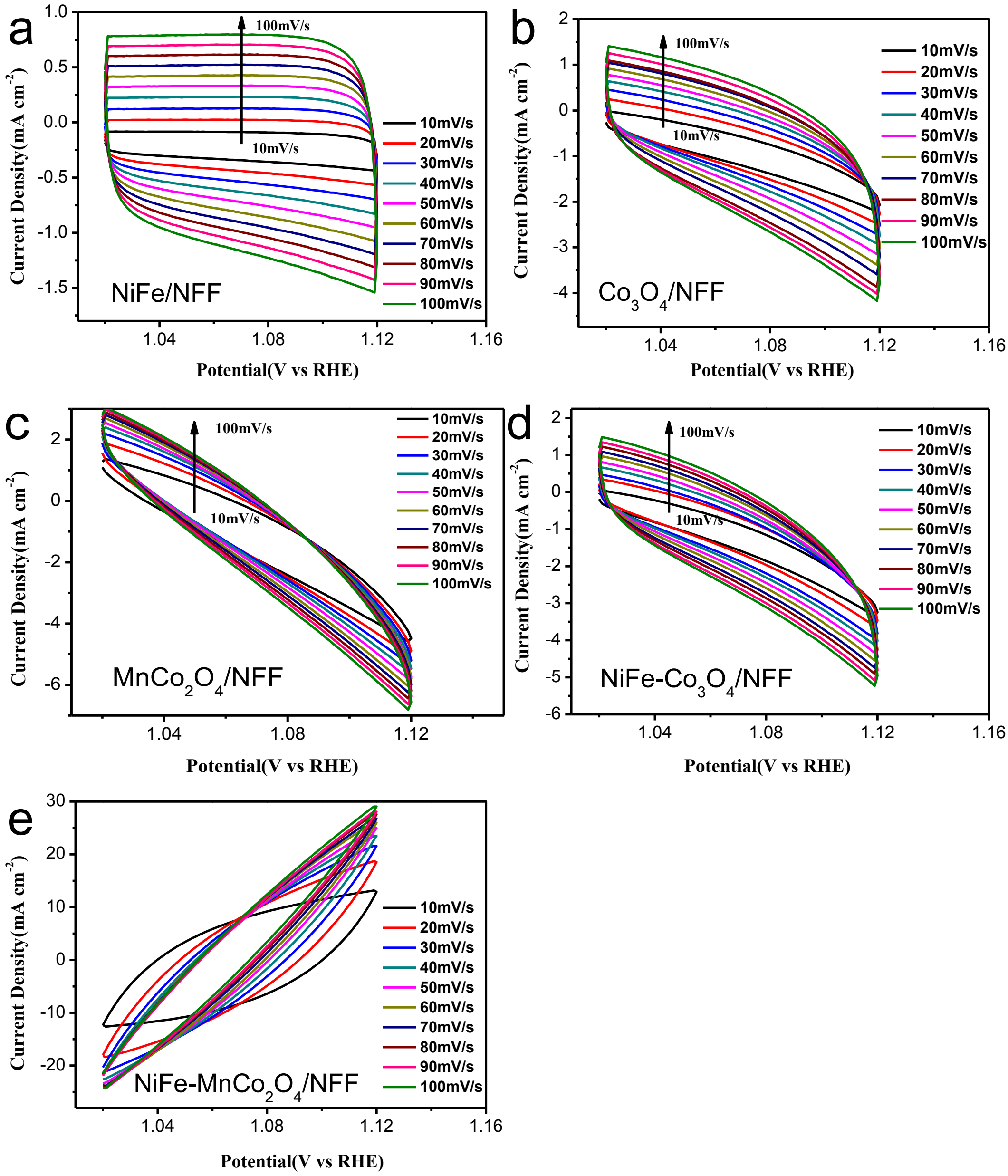

Fig. S6. The cyclic voltammograms (CVs) measurements for OER with various scan rates from 10 to 100 mV s^{-1} for (a) NiFe/NFF (b) Co_3O_4/NFF (c) $MnCo_2O_4$/NFF (d) NiFe-Co_3O_4/NFF (e) NiFe-$MnCo_2O_4$/NFF.

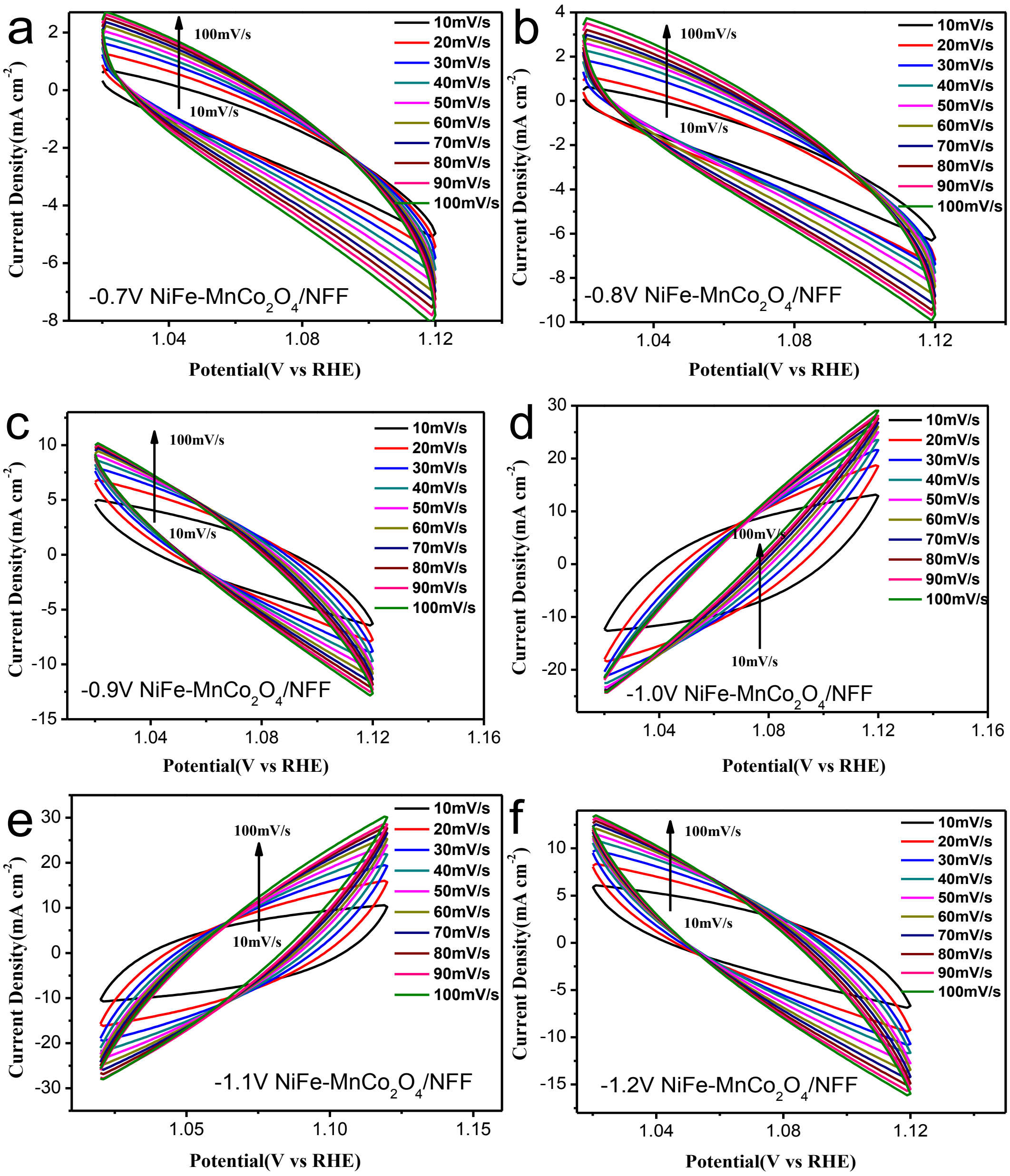

Fig. S7. The cyclic voltammograms (CVs) measurements for OER with various scan rates from 10 to 100 mV s^{-1} for (a) -0.7V NiFe-$MnCo_2O_4$/NFF (b) -0.8V NiFe-$MnCo_2O_4$/NFF (c) -0.9V NiFe-$MnCo_2O_4$/NFF (d) -1.0V NiFe-$MnCo_2O_4$/NFF (e) -1.1V NiFe-$MnCo_2O_4$/NFF (f) -1.2V NiFe-$MnCo_2O_4$/NFF

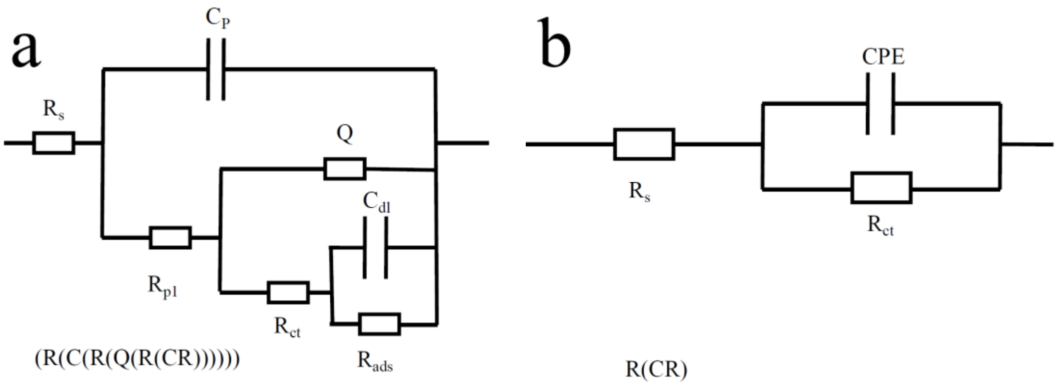

Fig. S8. The equivalent circuit diagram used for analysis of the EIS curves measured for the (a) OER and the (b) HER.

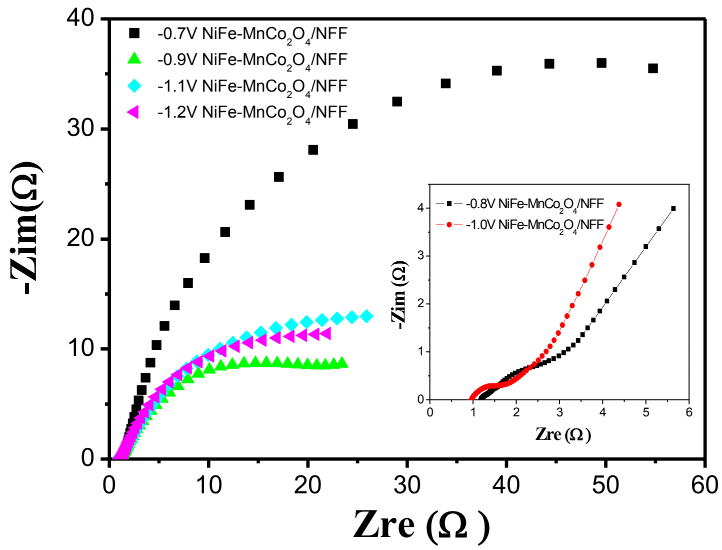

Fig. S9. EIS measured of as-deposited NiFe-$MnCo_2O_4$/NFF at varying depositing potential -0.7 V~ -1.2 V vs Ag/AgCl (at an overpotential of 300 mV in 1M KOH).

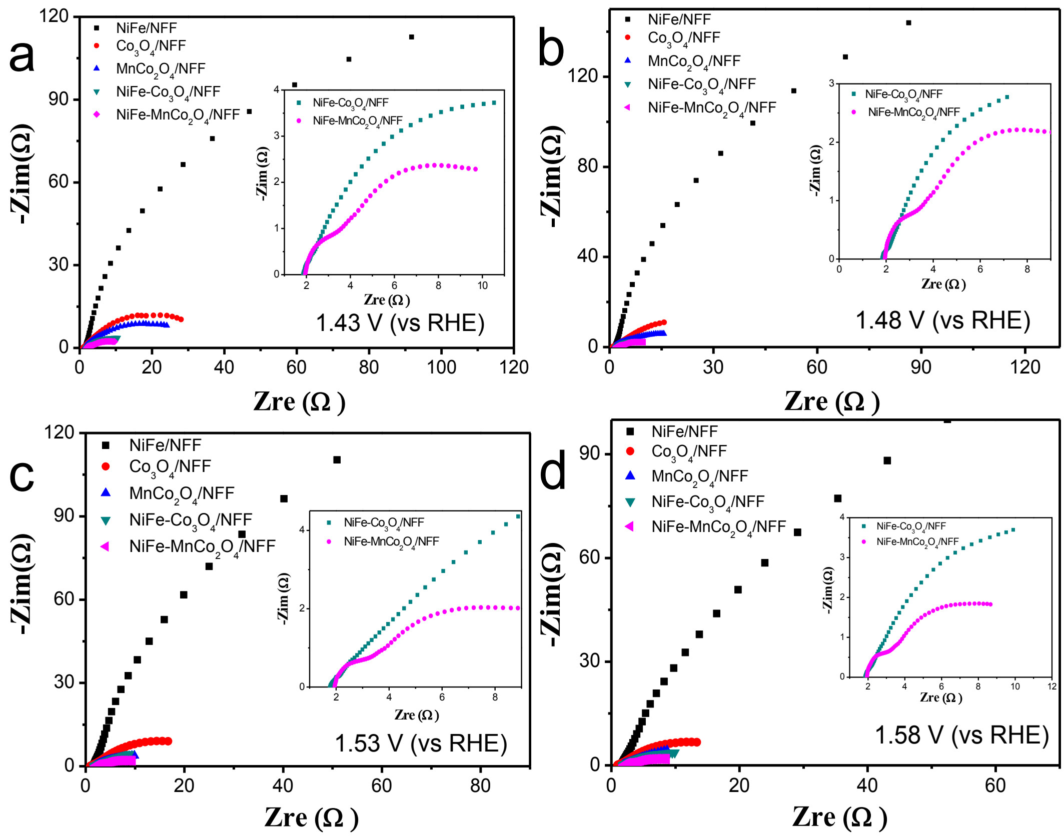

Fig. S10. Nyquist plots of NiFe/NFF, Co_3O_4/NFF, $MnCo_2O_4$/NFF, NiFe-Co_3O_4/NFF, and NiFe-$MnCo_2O_4$/NFF for OER tested at (a) 1.43, (b) 1.48, (c) 1.53, and (d) 1.58 V (vs RHE), respectively. The inset shows the enlarged EIS activity of the NiFe-Co_3O_4/NFF, and NiFe-$MnCo_2O_4$/NFF electrodes.

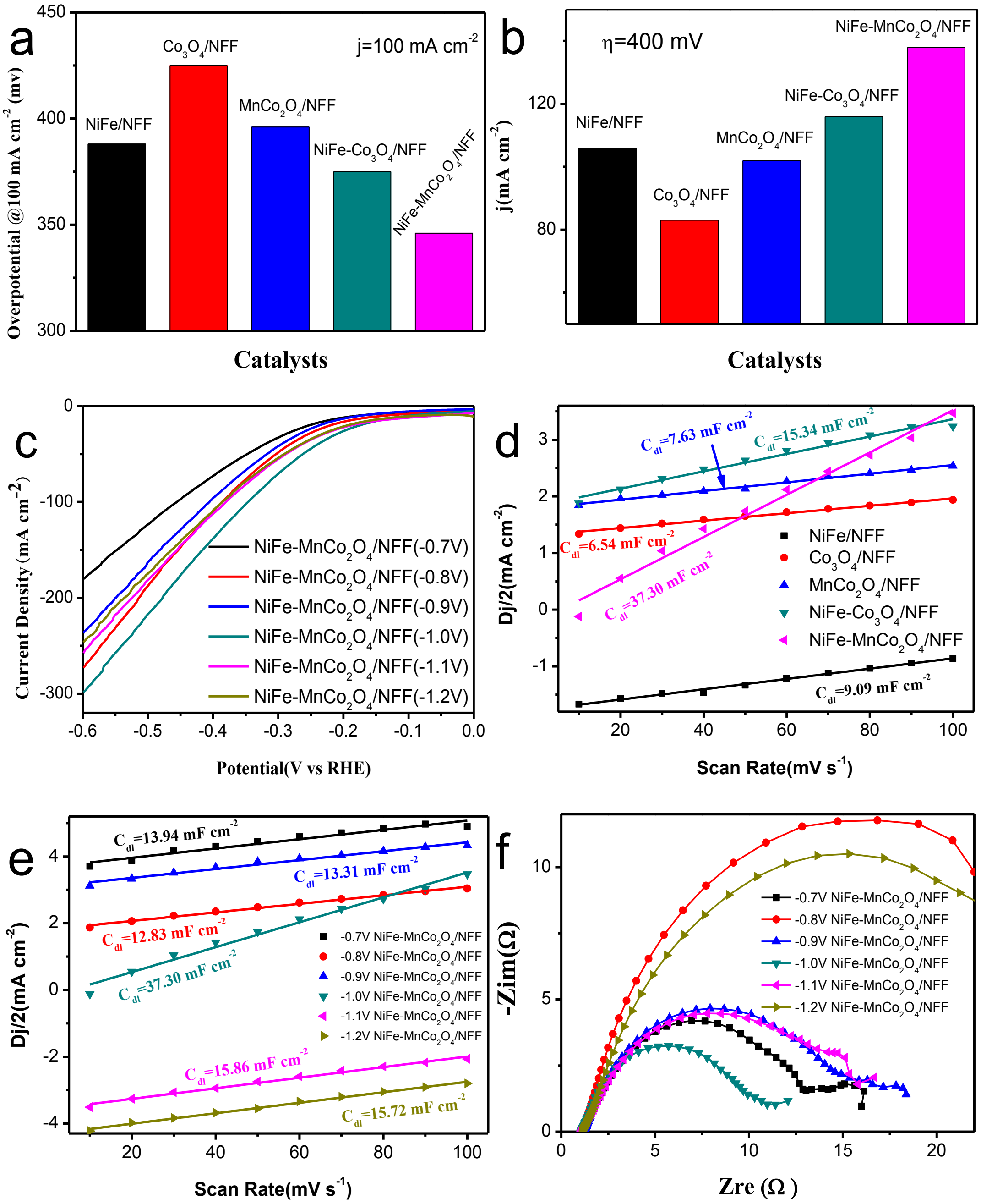

Fig. S11. HER (a) Overpotentials required for 100 mA cm^{-2}. (b) Current density at η = 400 mV for the different catalysts. (c) LSV curves for -0.7V NiFe-$MnCo_2O_4$/NFF, -0.8V NiFe-$MnCo_2O_4$/NFF, -0.9V NiFe-$MnCo_2O_4$/NFF, -1.0V NiFe-$MnCo_2O_4$/NFF, -1.1V NiFe-$MnCo_2O_4$/NFF, and -1.2V NiFe-$MnCo_2O_4$/NFF with a scan rate of 5 mV s^{-1} for the HER. (d) Capacitive currents of the catalysts with a scan rate of 10, 20, 30, 40, 50, 60, 70, 80, 90, and 100 mV s^{-1}. (e) Current density differences plotted against scan rates under a non-Faradaic range. (f) Current density differences plotted against scan rates under a non-Faradaic range.

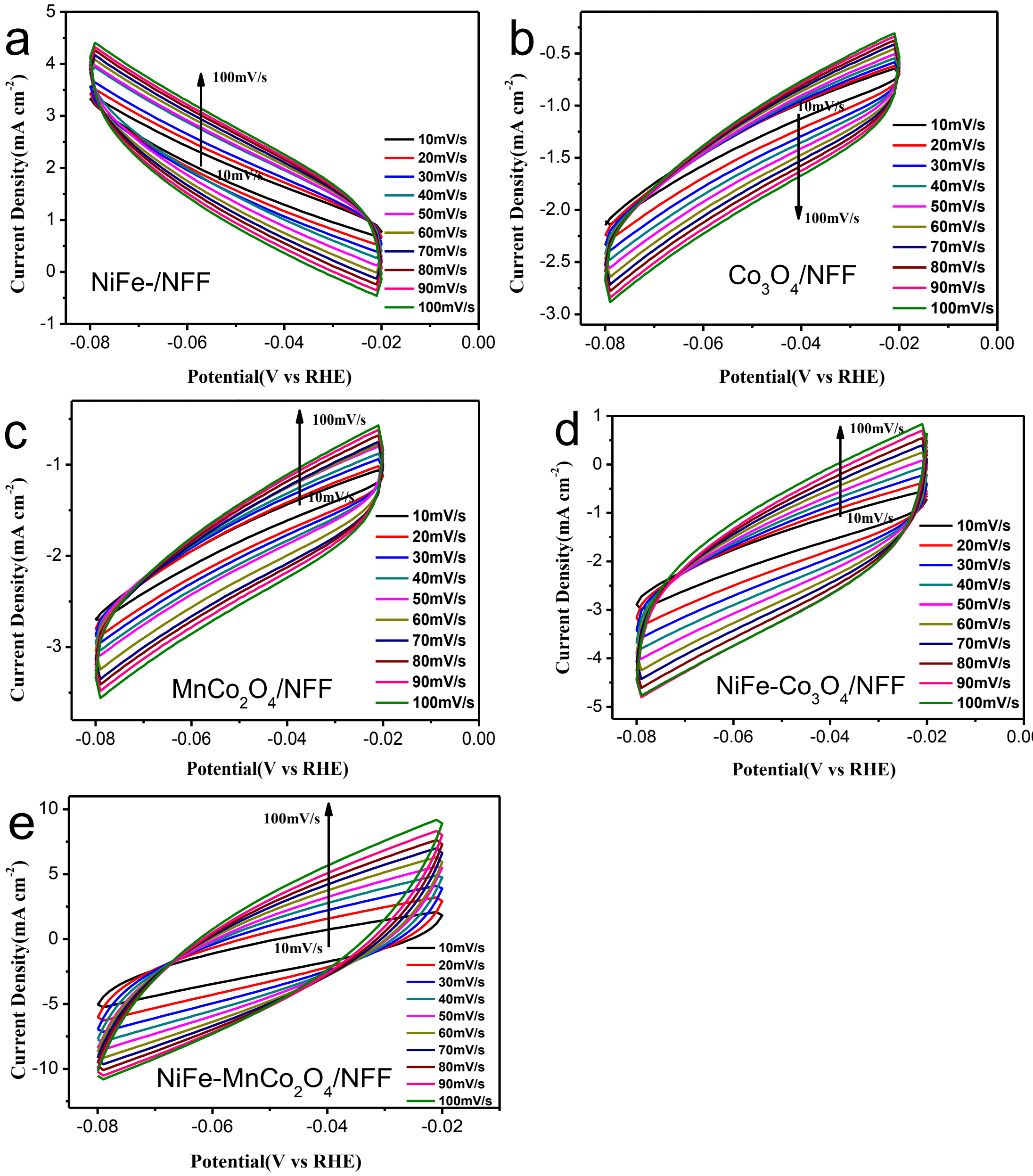

Fig. S12. Cyclic voltammograms (CVs) measurements for HER of (a) NiFe/NFF (b) Co_3O_4/NFF (c) $MnCo_2O_4$/NFF (d) NiFe-Co_3O_4/NFF (e) NiFe-$MnCo_2O_4$/NFF with different scan rates (10-100 mV s^{-1}) in the region from -1.08 to -1.02 vs RHE.

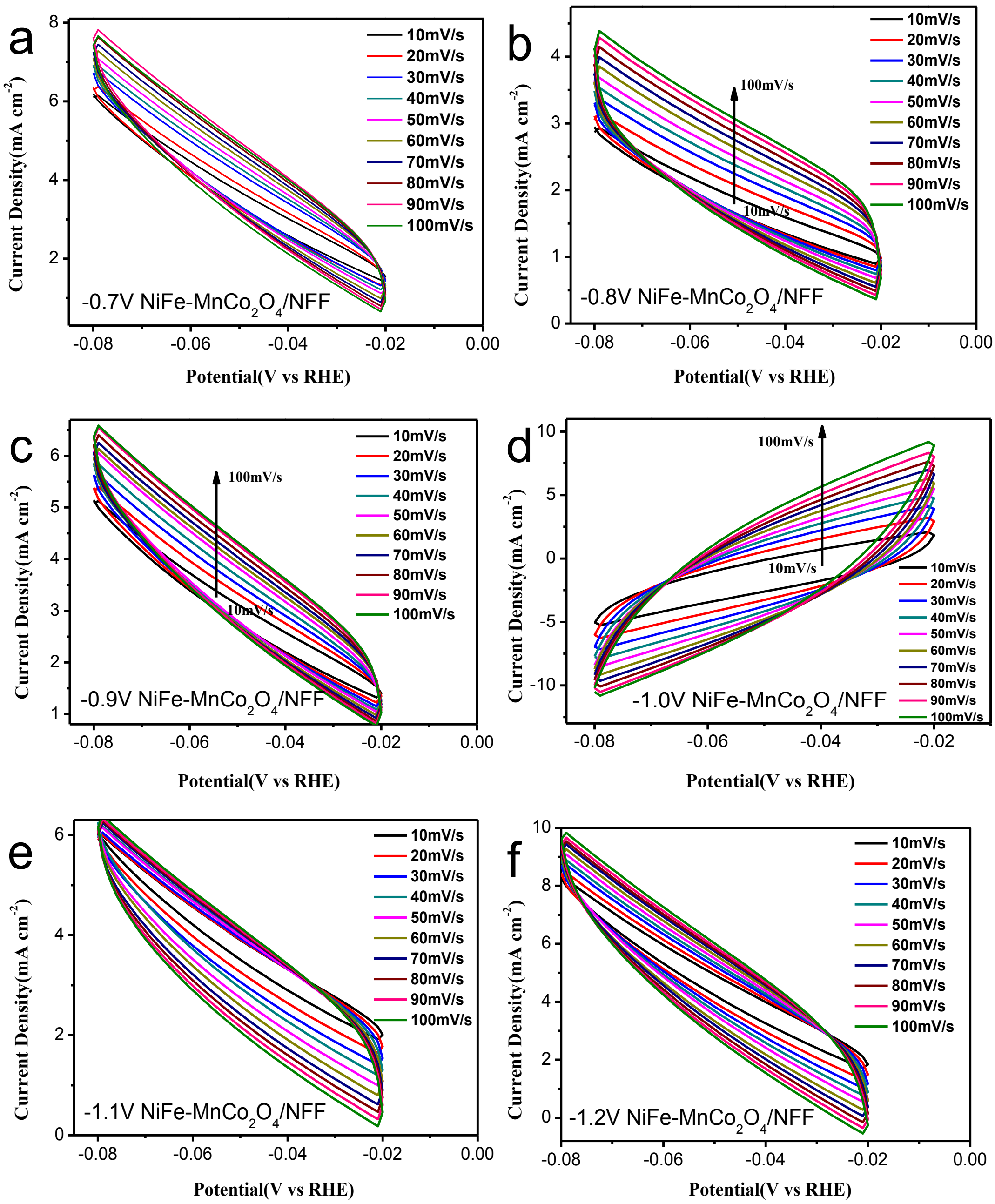

Fig. S13. Cyclic voltammograms (CVs) measurements for HER of (a) -0.7V NiFe-$MnCo_2O_4$/NFF (b) -0.8V NiFe-$MnCo_2O_4$/NFF (c) -0.9V NiFe-$MnCo_2O_4$/NFF (d) -1.0V NiFe-$MnCo_2O_4$/NFF (e) -1.1V NiFe-$MnCo_2O_4$/NFF (f) -1.2V NiFe-$MnCo_2O_4$/NFF with different scan rates (10-100 mV s^{-1}) in the region from -1.08 to -1.02 vs RHE.

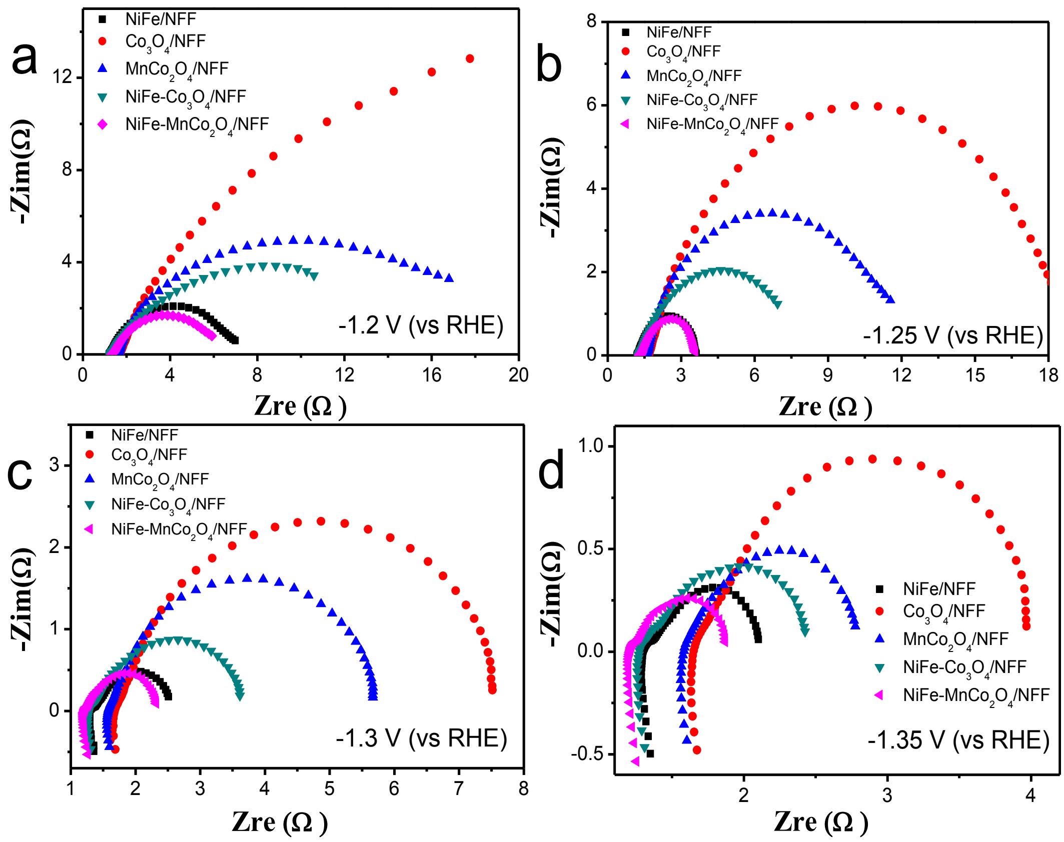

Fig. S14. Nyquist plots of NiFe/NFF, Co_3O_4/NFF, $MnCo_2O_4$/NFF, NiFe-Co_3O_4/NFF, and NiFe-$MnCo_2O_4$/NFF for HER tested at (a) -1.2, (b) -1.25, (c) -1.3, and (d) -1.35 V versus RHE, respectively.

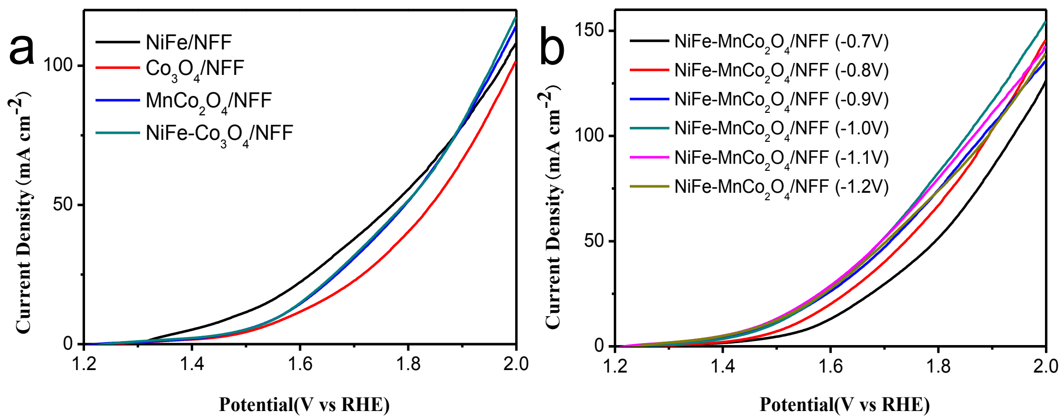

Fig. S15. (a) The polarization curves of NiFe/NFF, Co_3O_4/NFF, $MnCo_2O_4$/NFF, and NiFe-Co_3O_4/NFF catalysts in a two-electrode configuration. (b) The polarization curves of -0.7V NiFe-$MnCo_2O_4$/NFF, -0.8V NiFe-$MnCo_2O_4$/NFF, -0.9V NiFe-$MnCo_2O_4$/NFF, -1.0V NiFe-$MnCo_2O_4$/NFF, -1.1V NiFe-$MnCo_2O_4$/NFF, and -1.2V NiFe-$MnCo_2O_4$/NFF catalysts in a two-electrode configuration.

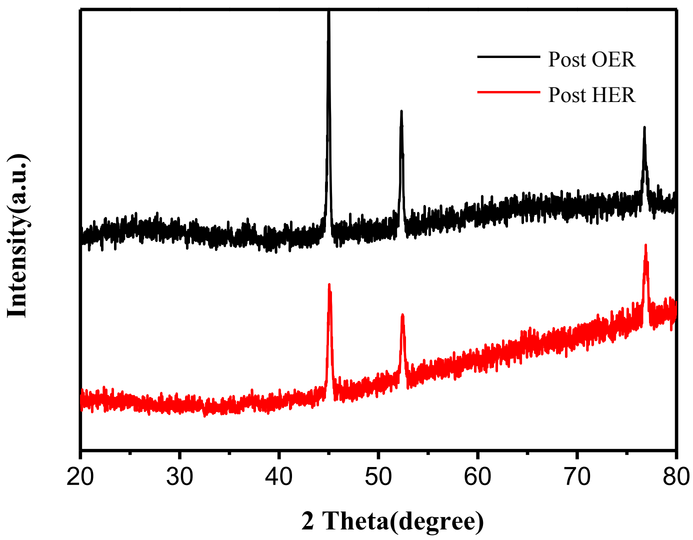

Fig. S16. XRD patterns of post-OER and post-HER of NiFe-$MnCo_2O_4$/NFF electrocatalysts.

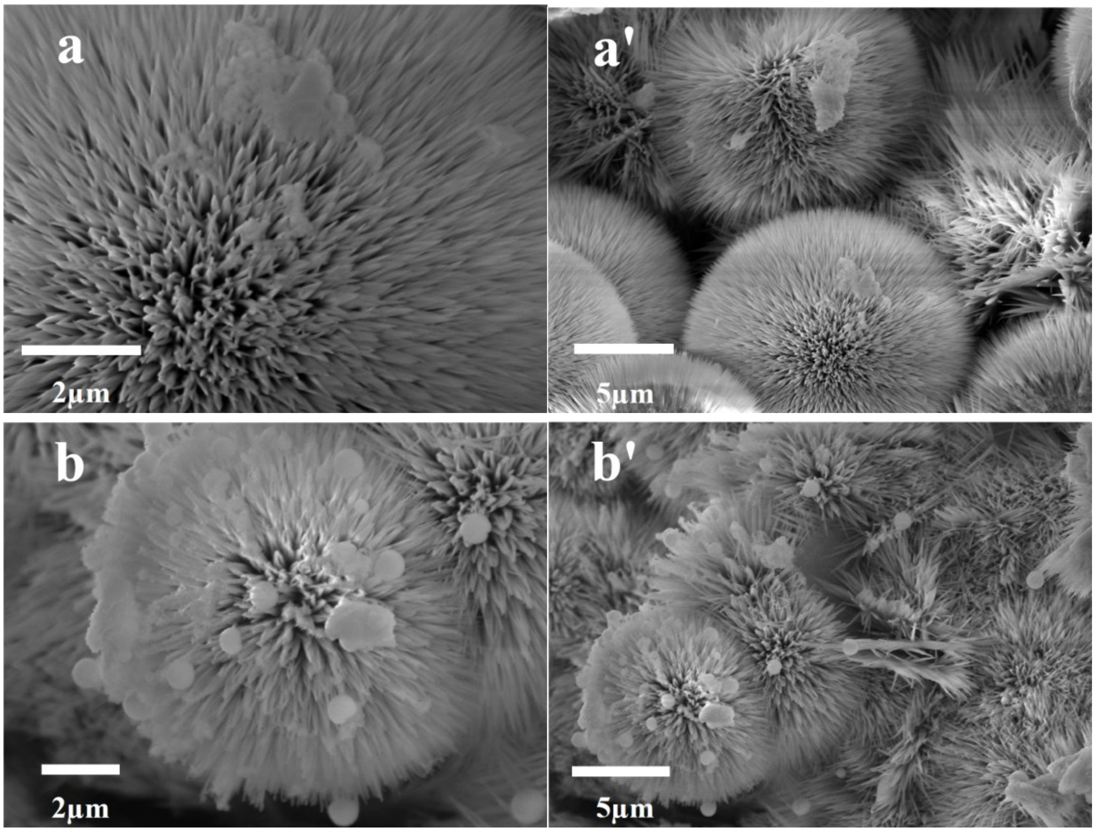

Fig. S17. The morphologies of NiFe-$MnCo_2O_4$/NFF after long-term (a and a') OER and (b and b') HER electrolysis.

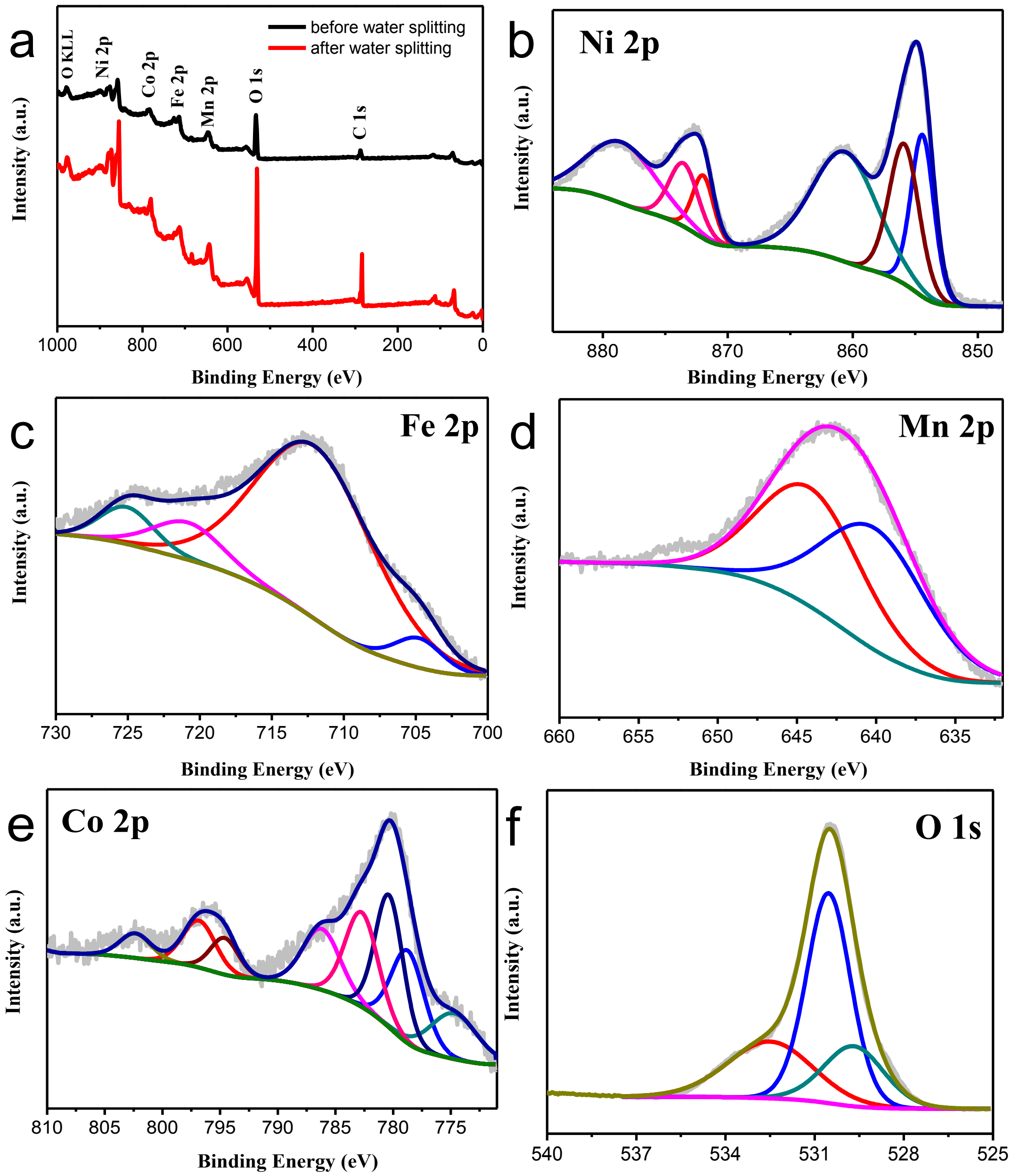

Fig. S18. The XPS spectra of NiFe-$MnCo_2O_4$/NFF (cathode) after overall water splitting stability test (a) survey (b) Ni 2p (c) Fe 2p (d) Mn 2p (e) Co 2p (f) O 1s regions.

Table S1 The ICP-AES analysis of the content of Ni and Fe for $MnCo_2O_4$/NFF and NiFe-$MnCo_2O_4$/NFF.

Composites	Atomic% Ni	Atomic% Fe	Element contant ratio of Ni : Fe (%)
$MnCo_2O_4$/NFF	87.624%	0.614%	142.71%
NiFe-$MnCo_2O_4$/NFF	88.199%	3.009%	29.31%

Table S2 Comparison of OER properties for electrocatalysts of catalytic materials

Electrode	**Electrolyte**	**η (mV)**	**Reference**
-1.0V NiFe-$MnCo_2O_4$/NFF	1 M KOH	272 mV@ 100 $mAcm^{-2}$	This work
NiFe/NFF	1 M KOH	349 mV@ 100 $mAcm^{-2}$	This work
Ru_2O/NFF	1 M KOH	387 mV@ 100 $mAcm^{-2}$	This work
Ir_2O/NFF	1 M KOH	457 mV@100 mA cm^{-2}	This work
NiFe/NF	1 M KOH	191 mV@ 10 $mAcm^{-2}$	*Electrochimica Acta*. **2019**, 299, 567-574
Ni-Fe LDH hollow Nanoprisms/NF	1 M KOH	280 mV@ 10 $mAcm^{-2}$	*Angew Chem Int Edit*. **2018**, 57, 172-176.
Fe-$Ni(OH)_2$/NF	1 M KOH	267 mV@ 10 $mAcm^{-2}$	*Chemical Communications* **2018**, 54, 463-466.
FeNi LDH/NF	1 M KOH	232 mV@ 10 $mAcm^{-2}$	*Angew Chem Int Edit.* **2014**, 53, 7584-7588-466.
NiFe LDH	1 M KOH	280 mV@ 10 $mAcm^{-2}$	*J Am Chem Soc.* **2014**, 136, 13118-21.
NiFeV LDHs	1 M KOH	192 mV@ 10 $mAcm^{-2}$	*Advanced Energy Materials* **2018**, 8(15), 1703341.
NiFe foam	1 M KOH	240 mV@ 10 $mAcm^{-2}$	*Int J Hydrogen Energ* **2015**, 40, 13258-63.
$Co_1Mn_1CH^*$	1 M KOH	322 mV@50 mA cm^{-2}	*J. Am. Chem. Soc.* **2017**, 139, 8320-8328.
NiFe/$NiCo_2O_4$/NF	1 M KOH	320 mV@600 mA cm^{-2}	*Adv. Funct. Mater.* **2016**, 26, 3515-3523.
NiFe-LDH/CNT	1 M KOH	250 mV@ 10 $mAcm^{-2}$	*J. Am. Chem. Soc.* **2013**, 135 , 8452
NiFe- rGO-LDH	1 M KOH	210 mV@ 10 $mAcm^{-2}$	*Angew. Chem.* **2014**, 126 , 7714 .
NiFe-NS	1 M KOH	300 mV@ 10 $mAcm^{-2}$	*Nat. Mater.* **2014**, 5 , 4477 .

Table S3 Comparison of HER properties for electrocatalysts of catalytic materials

Electrode	Electrolyte	η (mV)	Reference
NiFe-$MnCo_2O_4$/NFF	1 M KOH	98 mV@ 10 $mAcm^{-2}$	This work
PtC/NFF	1 M KOH	18 mV@ 10 $mAcm^{-2}$	This work
NiFe/$NiCo_2O_4$/NF	1 M KOH	105 mV@10 mA cm^{-2}	*Adv. Funct. Mater.* **2016**, 26, 3515-3523.
47.6% Pt/C	1 M KOH	40 mV@10 mA cm^{-2}	*J. Mater. Chem. A* **2015**, *3*, 20080.
Mn-CoP	1.0 M KOH	95 mV@ 10 $mAcm^{-2}$	*Catal. Sci. Technol.* **2018**, 8, 4407
Co_1Mn_1CH/NF	1 M KOH	180 mV@ 10 $mAcm^{-2}$	*J. Am. Chem. Soc* **2017** 139, 8320-8328.
NiFe LDH/Cu foam	1 M KOH	192 mV@ 100 $mAcm^{-2}$	*Environ. Sci.* **2017**, 10, 1820.
$NiCo_2O_4$/NiFe LDH	1 M KOH	192 mV@ 10 $mAcm^{-2}$	*ACS Appl. Mater. Interfaces.* **2017**, 9, 1488.
NCNT/Ni-$NiFe_2O_4$/Ni foam	1 M KOH	140 mV@ 10 $mAcm^{-2}$	*Catal. Sci. Technol.*, **2019**, 9, 1595-1601
NiFe LDH/NF	1 M KOH	210 mV@ 10 $mAcm^{-2}$	*Science*, **2014**, 345, 1593.
P-Co_3O_4	1 M KOH	120 mV@ 10 $mAcm^{-2}$	*Energ. Environ. Sci.* **2017**, 10, 2563-2569
$NiCo_2O_4$*	1 M KOH	110 mV@ 10 $mAcm^{-2}$	*Angew. Chem. Int. Ed.* **2016**, 55, 6290.

Table S4 Comparison of overall water splitting performance for the recently reported catalysts and ours.

Electrode	Electrolyte	η (mV)	Reference
NiFe-$MnCo_2O_4$/NFF	1 M KOH	1.49 V@ 10 $mAcm^{-2}$	This work
Co_1Mn_1CH	1 M KOH	1.68 V@ 10 $mAcm^{-2}$	*J. Am. Chem. Soc* **2017** 139, 8320-8328.
NiFe LDH/NF	1 M KOH	1.70 V@ 10 $mAcm^{-2}$	*Science*, **2014**, 345, 1593-1596.
$NiCo_2O_4$ hollow microcuboids	1 M KOH	1.65 V@ 10 $mAcm^{-2}$	*Angew. Chem., Int. Ed.*, **2016**, 55, 1-6.
CoMnO@CN	1 M KOH	~1.5 V@ 10 $mAcm^{-2}$	*J. Am. Chem. Soc*. **2015**, 13, 14305.
Ni_3FeN/r-GO	1 M KOH	1.60 V@ 10 $mAcm^{-2}$	*ACS Nano*. **2018**, 12, 245
Co_5Mo_1 Composite @Ni foam	1 M KOH	1.68 V@ 10 $mAcm^{-2}$	*Nano Energy*, **2018**, 45, 448-455.
Ni_2Fe_1-O	1 M KOH	1.64 V@ 10 $mAcm^{-2}$	*Adv. Energy Mater.* **2017**, 8, 1701347.
Cu@CoFe LDH	1 M KOH	1.68 V@ 10 $mAcm^{-2}$	*Angew. Chem. Int. Ed.* **2018**, 130, 178-182.
NiFe-LDH/$NiCo_2O_4$	1 M KOH	1.60V@ 10 mA cm^{-2}	*ACS Appl. Mater. Interfaces*. **2017**, 9, 15364-15372.
$Mo_{51}Ni_{40}Fe_9$	1 M KOH	1.55V@ 10 mA cm^{-2}	*ACS Catal.* **2019**, 9, 1013-1018.
NiS/NiS_2	1 M KOH	1.62V@ 10 mA cm^{-2}	*J. Mater. Chem. A*, **2018**, 6, 8233